Title

AcidoCEST-UTE MRI for the Assessment of Extracellular pH of Joint Tissues at 3 T.

Journal

Investigative radiology, 54(9)

ISSN

0020-9996

Authors

Ma, Ya-Jun
High, Rachel A
Tang, Qingbo
et al.

Publication Date

2019-09-01

DOI

10.1097/rli.0000000000000576

Peer reviewed

AcidoCEST-UTE MRI for the Assessment of Extracellular pH of Joint Tissues at 3 T

Ya-Jun Ma, PhD,† Rachel A. High, PhD,*† Qingbo Tang, PhD,*† Lidi Wan, MD,*† Saeed Jerban, PhD,*† Jiang Du, PhD,*† and Eric Y. Chang, MD*†*

Objectives: The goal of this study was to demonstrate feasibility of measuring extracellular pH in cartilage and meniscus using acidoCEST technique with a 3-dimensional ultrashort echo time readout (acidoCEST-UTE) magnetic resonance imaging (MRI).

Materials and Methods: Magnetization transfer ratio asymmetry, radiofrequency (RF) power mismatch, and relative saturation transfer were evaluated in liquid phantoms for iopromide, iopamidol, and iohexol over a pH range of 6.2 to 7.8, at various agent concentrations, temperatures, and buffer concentrations. Tissue phantoms containing cartilage and meniscus were evaluated with the same considerations for iopamidol and iohexol. Phantoms were imaged with the acidoCEST-UTE MRI sequence at 3 T. Correlation coefficients and coefficients of variations were calculated. Paired Wilcoxon rank-sum tests were used to evaluate for statistically significant differences.

Results: The RF power mismatch and relative saturation transfer analyses of liquid phantoms showed iopamidol and iohexol to be the most promising agents for this study. Both these agents appeared to be concentration independent and feasible for use with or without buffer and at physiologic temperature over a pH range of 6.2 to 7.8. Ultimately, RF power mismatch fitting of iohexol showed the strongest correlation coefficients between cartilage, meniscus, and fluid. In addition, ratiometric values for iohexol are similar among liquid as well as different tissue types.

Conclusions: Measuring extracellular pH in cartilage and meniscus using acidoCEST-UTE MRI is feasible.

Key Words: MRI, chemical exchange saturation transfer, pH, osteoarthritis, acidoCEST

(*Invest Radiol* 2019;54: 565–571)

Osteoarthritis is a common disease that has substantial impact on affected individuals, healthcare systems, and society as a whole.[1] Imaging is important for the diagnosis and management of osteoarthritis, and magnetic resonance imaging (MRI) is widely considered the most comprehensive modality for assessment of the joint.[2] Conventional clinical MRI is highly sensitive for gross morphological abnormities, such as chondral fissures or meniscal tears. Using more research-oriented, relaxation-based techniques, including T2, T2*, dGEMRIC, and T1ρ, more sensitive quantitative measurements can be made on joint tissues.[3] Of note, however, all of these methods either focus on or are strongly influenced by structural changes. Unfortunately, the reality is that once the collagen network is degraded, it has reached an irreversible state.[4] Furthermore, structural assessment can be limited due to its poor correlations with patient symptoms.[5] Development of imaging techniques that identify earlier changes or provide complementary information that may improve correlations with patient symptoms would be highly beneficial.

It is now widely accepted that osteoarthritis is not just a structural wear-and-tear disease, but an active, biochemically mediated process.[6] An important component of normal physiology and tissue function is acid-base homeostasis and pH regulation. For instance, degradation of the extracellular matrix of cartilage is orchestrated by matrix metalloproteinases and a disintegrin and metalloproteinase with thrombospondin type I motifs.[7] Expression and function of several of these proteins are influenced by extracellular pH (pHe).[8,9] In addition, aberrant neurovascular invasion at the osteochondral junction is mediated by osteoclasts, which dissolve mineral by massive acid secretion.[10,11] The nociceptors in these osteochondral channels and in osteoarthritic menisci can be either directly activated or sensitized by protons through acid-sensing ion channels.[12,13]

Recently, pHe-sensitive MRI has been performed with chemical exchange saturation transfer (CEST) after administration of Food and Drug Administration– and European Medicines Agency–approved contrast agents typically used with computed tomography (CT), termed acidoCEST MRI.[14] AcidoCEST measures the CEST signals produced by the exchange of protons between amide side chains and water. The CEST signal is linearly correlated with pH because the exchange is base-catalyzed.[15] Evaluation of tissue pH using acidoCEST has primarily focused on oncologic applications[16,17] and has not yet been used on diarthrodial joint tissues. Furthermore, readouts used with acidoCEST have included gradient sequences (spoiled or steady-state), fast-spin echo (FSE), or echo planar imaging, all with typically longer echo times. These techniques would be less optimal for musculoskeletal tissues with short transverse relaxation times, such as deep layers of cartilage when oriented parallel to B_0[18,19] and menisci, for which ultrashort echo time (UTE) sequences would be more ideal.[20]

The purpose of our study was to show feasibility of measuring pHe in cartilage and menisci using the acidoCEST technique with a 3-dimensional (3D) UTE readout (acidoCEST-UTE) on a 3 T clinical scanner. Toward this goal, numerous experimental variables were investigated, including (1) those related to the solution (contrast agent, concentration, presence of buffer, and temperature), (2) those related to the sequence (saturation power), and (3) those related to signal processing (ratiometric analysis based on saturation transfer [ST] or radiofrequency [RF] power).

MATERIALS AND METHODS

This phantom and ex vivo study was exempted from institutional review board approval.

Chemicals

Commercially purchased stock solutions of iopamidol at 972 mM concentration (370 mg I/mL Isovue; Bracco Imaging S.p.A, Milan, Italy), iopromide at 972 mM concentration (370 mgI/mL Ultravist; Bayer Healthcare Pharmaceuticals LLC, Berlin, Germany), and iohexol at

Received for publication January 31, 2019; and accepted for publication, after revision, April 3, 2019.

From the *Department of Radiology, University of California, San Diego Medical Center; and †Radiology Service, VA San Diego Healthcare System, San Diego, CA.

Drs Ya-Jun Ma and Rachel High contributed equally to this work.

Conflicts of interest and sources of funding: The authors gratefully acknowledge grant support from the VA Rehabilitation Research and Development Service. (Merit Award I01RX002604), VA Clinical Science Research and Development Service (Merit Award I01CX001388), and National Institutes of Health (2R01AR062581, 1R01AR068987, and 1R21AR073496).

The authors declare no conflicts of interest.

Supplemental digital contents are available for this article. Direct URL citations appear in the printed text and are provided in the HTML and PDF versions of this article on the journal's Web site (www.investigativeradiology.com).

Correspondence to: Eric Y. Chang, MD, Radiology Service, VA San Diego Healthcare System, 3350 La Jolla Village Drive, MC 114, San Diego, CA 92161. E-mail: ericchangmd@gmail.com.

ISSN: 0020-9996/19/5409–0565

DOI: 10.1097/RLI.0000000000000576

920 mM concentration (350 mgI/mL Omnipaque; GE Healthcare, Chicago, IL) were used in this study. All other chemicals were purchased from Sigma-Aldrich (St Louis, MO).

Phantom Preparation

An initial set of samples was prepared with all 3 contrast agents at 50 and 200 mM concentrations using either concentrated phosphate-buffered saline (PBS) to achieve a final concentration of 10 mM of PBS or normal saline without buffer. For each condition, pH of samples was varied between 6.2 and 7.8 as measured with a calibrated pH electrode (LE422, FiveEasy F20 bench meter; Mettler Toledo, Columbus, OH). To further assess the effects of buffer, phantoms were created using iopamidol or iohexol and phosphate-buffered saline to achieve 200 mM final contrast concentration and 5, 10, 20, and 40 mM final concentrations of phosphate-buffered saline for pH 6.6 and 7.2. A second set of phantoms was created using iopamidol and iohexol and concentrated phosphate-buffered saline to achieve 30 to 300 mM contrast concentration and 10 mM final concentration of phosphate-buffered saline at pH values of 6.6 and 7.2. A third set of ex vivo cartilage and menisci tissue phantoms were created using iopamidol and iohexol between 100 to 400 mM concentration and 10 mM final concentration of phosphate-buffered saline at pH values ranging between 6.2 and 7.8. Only grossly normal tissues were used in this study, harvested from 4 male donors (31, 53, 54, and 80 years of age at death). In brief, coins of pure cartilage were created from osteochondral cores, all from various locations within the joint. Menisci slices were also harvested. Tissues were soaked in the solution for at least 96 hours, and solutions and tissue surface pH values were tested using an electrode (LE427 solid tissue electrode, FiveEasy F20 bench meter; Mettler Toledo, Columbus, OH) after scanning to ensure pH stability. All phantoms were cylindrical in shape, either in sealed plastic transfer pipette heads or syringes. These phantoms were then placed into a cylindrical container filled with Fomblin (Ausimont, Thorofare, NJ) and scanned parallel to B_0 at isocenter to minimize susceptibility. All 3 sets of phantoms were scanned at both 23°C and at physiologic temperature (35°C), which was maintained using an MRI-compatible, regulated air heater that was created in-house with a hair-dryer fan, insulated hoses, fiber optic sensors, and a Styrofoam box. Temperatures inside of the box were tested and could be maintained within ±0.2°C for over 4 hours.

Magnetic Resonance Imaging

All imaging was performed on a 3 T clinical scanner (MR750, GE Healthcare, Milwaukee, WI) using an 8-channel transmit/receive knee coil. The 3D UTE sequence using spiral trajectories with conical view ordering was used for the readout.[21,22] For the liquid phantom scans, the 3D acidoCEST-UTE sequence (Fig. 1) parameters used were as follows: TR = 62 milliseconds, TE = 0.032 milliseconds, number of spokes (N_{sp}) = 5, spoke interval (τ) = 5 milliseconds, flip angle (FA) = 5 degrees, BW = 166 kHz, field of view = 12 × 12 × 11.2 cm^3, and matrix = 160 × 160 × 28. Chemical exchange saturation transfer contrast was created with a Fermi pulse: duration = 32 milliseconds, bandwidth = 40 Hz, B_1s = 0.54 (300 degrees) and 1.1 μT (600 degrees) as calculated by power average,[23] 55 frequency offsets from −1080 to 1080 Hz in 40 Hz increments, with 1 minute and 10 seconds of scan time per frequency. Steady-state before acquisition was achieved using an 8-second dummy scan. For the ex vivo cartilage and meniscus phantom scans, the sequence parameters were identical to the liquid phantoms except for higher resolution (field of view = 12 × 12 × 14.4 cm^3, matrix = 160 × 160 × 48) and resultant 2-minute scan time per frequency. Three-dimensional FSE images were also obtained using higher in-plane resolution at 256 × 256, TR = 1600 milliseconds, and TE = 40 milliseconds to improve visibility of tissue structures and boundaries. To correct for B_0 inhomogeneity, a dual-echo UTE sequence with TEs = 0.032 and 2.2 milliseconds were used to generate the B_0 map with other sequence parameters including FA = 8 degrees, TR = 20 milliseconds, and half in-plane resolution and same through-plane resolution as the CEST sequence.

Data Analysis

All data were processed using a home-developed MATLAB code (The Mathworks, Inc, Natick, MA, R2016b). Each frequency-offset datum was smoothed using a 3D Gaussian kernel with standard deviation of 0.8. The Z-spectrum was then obtained by interpolating the frequency-offset data points with splines to determine the exact

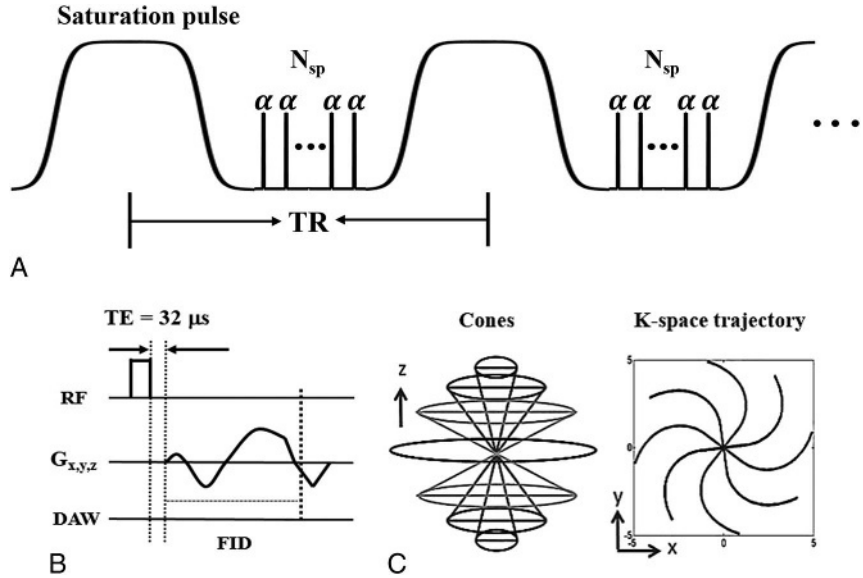

FIGURE 1. The acidoCEST-UTE sequence. A Fermi pulse was used to create CEST contrast followed by the multiple spokes (N_{sp}) excitation to accelerate the scan (A). Each excitation uses a short rectangular pulse (duration = 16 μs) for signal excitation (B), followed by a 3D Cones trajectory to allow time-efficient sampling with a minimal TE of 32 μs (C). Data acquisition window (DAW) starts at the beginning of the readout gradient. TR indicates repetition time; TE, echo time; RF, radiofrequency; $G_{x,y,z}$, gradient in x,y,z directions; FID, free induction decay.

locations of the frequency offsets of bulk water and CEST peaks (ie, 0, 4.2, 4.3, and 5.6 ppm). All data were then corrected by frequency shifting based on the measured B_0 maps. The magnetization transfer ratio asymmetry (MTR_{asym}) was calculated by:

$$MTR_{asym}(\Delta w) = \frac{I(-\Delta w) - I(\Delta w)}{I_0} \times 100, \quad [1]$$

where Δw is the frequency offset. $I(\Delta w)$ and $I(-\Delta w)$ are the signal intensities at the frequency offsets of Δw and $-\Delta w$, respectively. I_0 is the signal intensity without the saturation pulse. Moreover, the ST was determined by

$$ST(\Delta w) = \frac{I(-\Delta w) - I(\Delta w)}{I(-\Delta w)} \times 100. \quad [2]$$

Based on the obtained MTR_{asym} and ST values, the ratio of the RF power mismatch (RPM)[24] and the relative saturation transfer (RST)[25] can be determined by

$$RPM(\Delta w) = \frac{\left[\left(100 - MTR_{asym}(\Delta w)\right)/MTR_{asym}(\Delta w)\right]_{RF1}}{\left[\left(100 - MTR_{asym}(\Delta w)\right)/MTR_{asym}(\Delta w)\right]_{RF2}} \quad [3]$$

and

$$RST(\Delta w) = \frac{\left[\left(100 - ST(\Delta w)\right)/ST(\Delta w)\right]_{peak1}}{\left[\left(100 - ST(\Delta w)\right)/ST(\Delta w)\right]_{peak2}}, \quad [4]$$

respectively. The index RF 1 and RF 2 refer to 2 different RF powers at the same CEST peak. Peak 1 and peak 2 refer to 2 different CEST peaks at the same power. For the RPM calculations for all the CEST peaks in iopromide (4.2 and 5.6 ppm), iopamidol (4.2 and 5.6 ppm), and iohexol (4.3 ppm), the FA of RF 1 is lower than that of RF 2. For the RST calculations of iopromide and iopamidol, the frequency offsets of peak 1 and peak 2 are 5.6 ppm and 4.2 ppm, respectively.

Statistical Analysis

Statistical calculations were performed using SPSS (SPSS version 21; SPSS, Chicago, IL). The paired Wilcoxon rank-sum test was used to evaluate for statistically significant differences between MTR_{asym} for each of the contrast agents with or without added buffer and at when scanned at 23°C and 35°C. *P* values less than 0.05 were considered statistically significant. The coefficient of variation for the iopamidol and iohexol with 0 to 40 mM buffer was calculated as CoV = standard deviation/mean.

RESULTS

Iopamidol and iopromide both carry unique amide groups, which produce CEST effects at 4.2 and 5.6 ppm (Fig. 2, A and E), whereas iohexol contains one amide group that produces CEST effect at 4.3 ppm (Fig. 2I). A comparison between the 3 agents at 200 mM contrast concentration, pH 6.3, and at 35°C highlights Z-spectra differences, with notable increases in MTR_{asym} as FA increases from 0.54 to 1.1 μT (Fig. 2, B, F, and J). From pH 6.2 to 7.8 at 35°C, MTR_{asym} ranges for iopromide at 0.54 μT were 3.32 to 9.24 at 4.2 ppm and 0.68 to 2.0 at

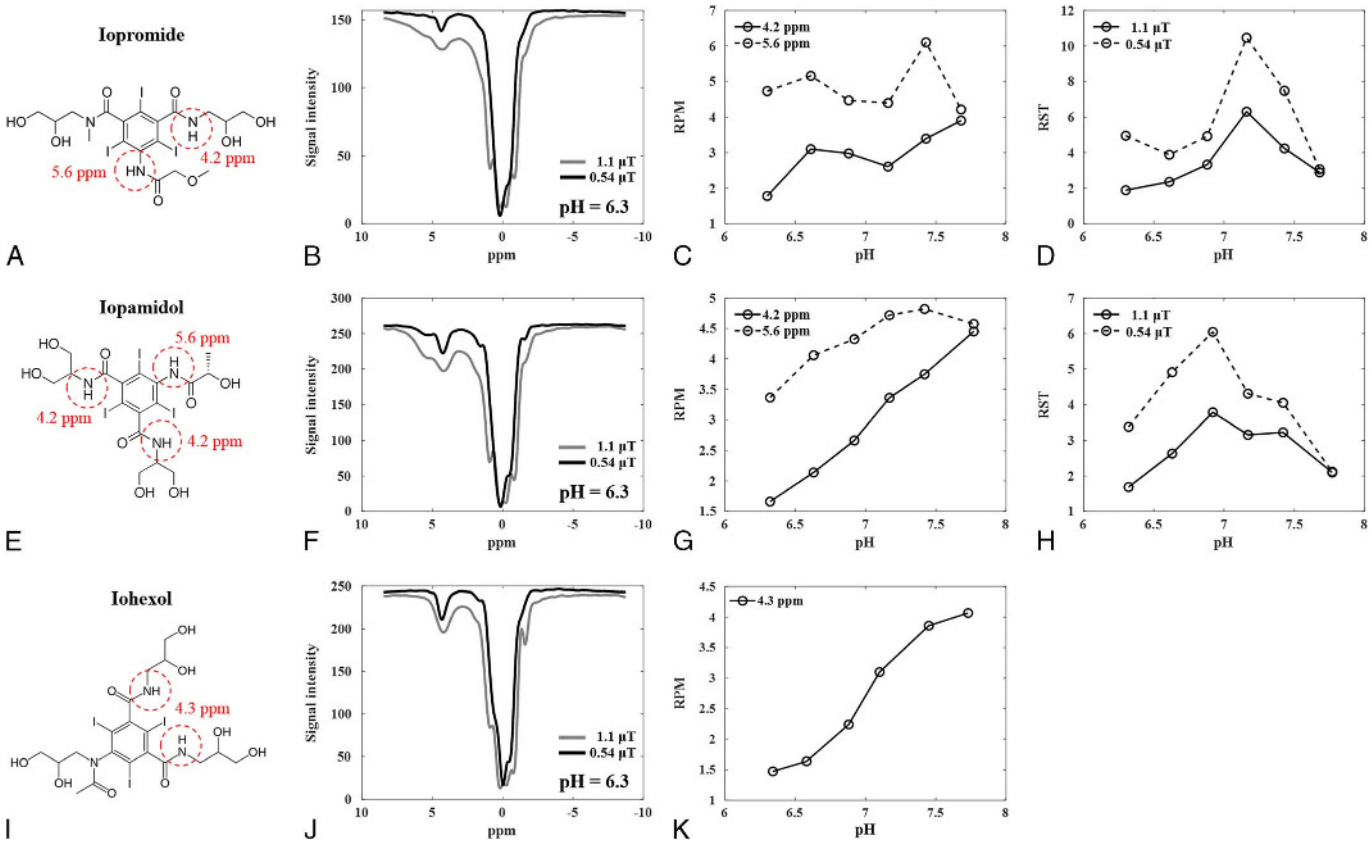

FIGURE 2. Comparison between iopromide, iopamidol, and iohexol at 35°C. The first row shows the chemical structure (A), Z-spectrum at pH = 6.3 (B), RPM values at both 4.2 and 5.6 ppm (C), and RST values at both 0.54 and 1.1 μT (D) for iopromide. The second row shows the chemical structure (E), Z-spectrum at pH = 6.3 (F), RPM values at both 4.2 and 5.6 ppm (G), and RST values at 0.54 and 1.1 μT (H) for iopamidol. The third row shows the chemical structure (I), Z-spectrum at pH = 6.3 (J), and RPM values at 4.3 ppm (K) for iohexol. RPM indicates ratio of RF power mismatch; RST, relative saturation transfer; ppm, parts per million.

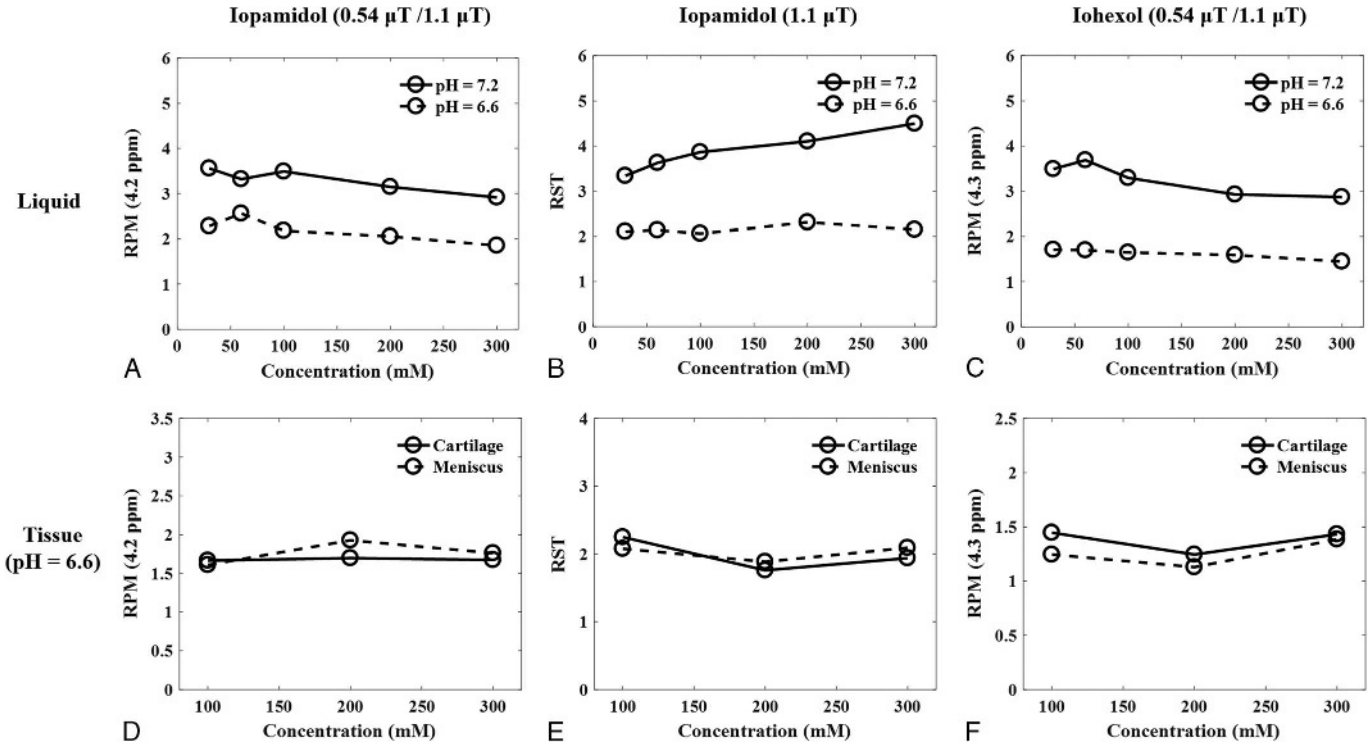

FIGURE 3. Investigation of CEST effects versus contrast agent concentrations for both liquid and tissue phantoms at 35°C. The first row shows the RPM values at 4.2 ppm for iopamidol (A), RST values at 1.1 μT for iopamidol (B), and RPM values at 4.3 ppm for iohexol (C) of the liquid phantom with 2 pH values of 6.6 and 7.2. The concentrations of both iopamidol and iohexol liquid phantom range from 30 to 300 mM. The second row shows the RPM values at 4.2 ppm for iopamidol (D), RST values at 1.1 μT for iopamidol (E), and RPM values at 4.3 ppm for iohexol (F) of the tissue phantom including both cartilage and meniscus at pH 6.6. The concentrations of both the iopamidol and iohexol tissue phantoms range from 100 to 300 mM. RPM indicates ratio of RF power mismatch; RST, relative saturation transfer; ppm, parts per million; mM, millimolar.

5.6 ppm, and at 1.1 μT were 11.84 to 15.93 at 4.2 ppm and 2.96 to 8.83 at 5.6 ppm. For iopamidol at 35°C, MTR_{asym} ranges at 0.54 μT were 3.14 to 15.49 at 4.2 ppm and 1.52 to 5.14 at 5.6 ppm, and at 1.1 μT were 12.62 to 30.62 at 4.2 ppm and 6.59 to 15.41 at 5.6 ppm. For iohexol at 35°C, MTR_{asym} ranges at 4.3 ppm were 4.05 to 13.08 at 0.54 μT and 14.66 to 25.77 at 1.1 μT. For iopromide, RPM for these 2 FAs yielded better performance for the 4.2 ppm peak compared with the 5.6 ppm peak (Fig. 2C). For iopamidol, the RPM for the 4.2 ppm peak performed better than the 5.6 ppm peak (Fig. 2G). For iohexol, the 4.3 ppm peak showed good performance (Fig. 2K). Of the 3 agents, RPM for the 4.2 ppm peak using iopamidol showed the most linear relationship with pH. RST did not perform well for iopromide (Fig. 2D) or iopamidol (Fig. 2H). Based on these data, iopamidol and iohexol were selected for use in the subsequent phantom studies, so as to include 1 agent with 2 CEST peaks and 1 with 1 CEST peak. Iopamidol was selected over iopromide due to having a larger maximal CEST effect over the tested pH range (30.62 vs 15.93, respectively, for the 4.2 ppm peak at 1.1 μT irradiation). Subsequent tests with iopamidol focused on RPM at the 4.2 ppm peak, as this showed a more linear relationship to pH than the 5.6 ppm peak or with RST analysis.

Varying contrast agent concentration from 50 to 300 mM in liquid phantoms had no notable effect on RPM at 4.2 ppm for pH 6.6 or 7.2 using iopamidol (Fig. 3A) or iohexol (Fig. 3C). Relative saturation transfer of iopamidol at pH 6.6 and 7.2 were likewise not notably affected over the same range of concentrations (Fig. 3B). Similar results were obtained using phantoms containing cartilage and meniscus samples in a pH 6.6 solution at a range of concentration from 100 to 300 mM (Fig. 3, D–F).

With regards to the effect of buffer at 23°C, a paired Wilcoxon rank-sum test showed that there was no significant difference in MTR_{asym} for 200 mM of iopamidol with or without added 10 mM buffer for pH 6.2 to 7.8 at the 4.2 ppm peak using B_1 values of 0.54 μT ($P = 0.345$) and 1.1 μT ($P = 0.255$), or at the 5.6 ppm peak at 0.54 μT ($P = 0.225$) and 1.1 μT ($P = 0.893$). Similarly, a Wilcoxon rank-sum test showed that there was no significant difference in MTR_{asym} for 200 mM of iohexol with or without added buffer for pH 6.2 to 7.8 at 0.54 μT ($P = 0.138$) and 1.1 μT ($P = 0.080$) at 23°C. Assessment of 200 mM of iopamidol with 0 to 40 mM phosphate-buffered saline at 35°C demonstrated a 3.9% to 13.2% CoV for RPM at 5.6 ppm (Supplementary Fig. 1A, Supplemental Digital Content 1, http://links.lww.com/RLI/A437) and 6.8% to 12.8% at 4.2 ppm (Supplementary Fig. 1B, Supplemental Digital Content 1, http://links.lww.com/RLI/A437). Assessment of 200 mM of iohexol with 0 to 40 mM phosphate-buffered saline at 35°C demonstrated a 5.9% to 7.5% CoV for RPM at 4.3 ppm (Supplementary Fig. 1C, Supplemental Digital Content 1, http://links.lww.com/RLI/A437).

For iopamidol, a paired Wilcoxon rank-sum test showed that overall CEST effects increased from room temperature to physiologic temperature (35°C) for the 4.2 ppm peak at 1.1 μT ($P = 0.005$), although no significant difference was detected at 0.54 μT ($P = 0.386$). For the 5.6 ppm peak of iopamidol, a paired Wilcoxon rank-sum test showed that CEST effects decreased at both 0.54 μT ($P = 0.017$) and 1.1 μT (0.047). A paired Wilcoxon rank-sum test showed that overall CEST effects for iohexol decreased at 1.1 μT ($P = 0.005$), although no significant difference was detected at 0.54 μT ($P = 0.241$).

Phosphate-buffered phantoms containing 200 mM of contrast and samples of cartilage and meniscus were evaluated over a pH range of 6.2 to 7.8, and fit of each curve from tissue was compared with the fit of the fluid portion of the respective phantom. RF power mismatch of iopamidol was evaluated at 4.2 ppm (Fig. 4A), as well as RST at 1.1 μT

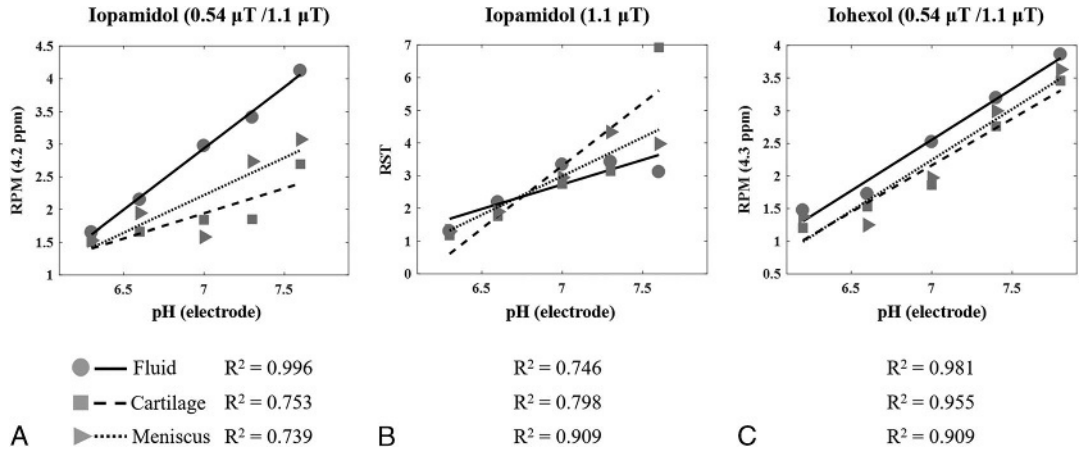

FIGURE 4. Comparison of CEST effects of fluid, cartilage, and meniscus in the tissue phantom with 200 mM of contrast at 35°C. RPM values at 4.2 ppm for iopamidol (A), RST values at 1.1 μT for iopamidol (B), and RPM values at 4.3 ppm for iohexol (C) for fluid, cartilage, and meniscus are presented with circles, squares, and triangles, respectively. The corresponding linear regression curves are shown with the measured R^2 values in the bottom row. RPM indicates ratio of RF power mismatch; RST, relative saturation transfer.

(Fig. 4B). RF power mismatch of iohexol was evaluated at 4.3 ppm (Fig. 4C) and shows superior correlations between fluid, cartilage, and meniscus. Notably, the slope and intercepts between fluid and tissues are the most similar for iohexol. Figure 5A shows the composition of the tissue phantoms, and Figure 5B shows a representative FSE image that was used to delineate the boundaries of cartilage and meniscus to facilitate ROI selection for analysis. Pixel maps of pH were generated for the iohexol phantoms using the fluid fit as a calibration curve, with the equation $y = 1.56 \times -8.39$ (Fig. 5C). The pH of fluid within each phantom was confirmed with a pH meter before and after scanning. Based on the MTR_{asym} values in the cartilage and menisci after 96 hours of soaking in 200 mM solution, contrast concentrations reached ~100 mM in the tissue.

DISCUSSION

In this study, we investigated the capability of the acidoCEST-UTE technique to measure pHe in liquid phantoms and ex vivo cartilage and menisci phantoms using a 3 T clinical scanner. Assessment of joint tissue pHe may have considerable significance, but has only been previously performed using highly invasive electrodes during open joint surgery.[9] The results from our study suggest that bathing the joint tissues with Food and Drug Administration– and European Medicines Agency–approved iodinated contrast agents (specifically iohexol or iopamidol), allowing sufficient time for contrast diffusion into the tissues, and subsequent scanning with the acidoCEST-UTE technique may be an alternative method to electrode testing for measurement of pHe. Of note, intra-articular injection of contrast is minimally invasive and routinely performed in clinical practice (eg, conventional radiographic, CT, or MR arthrography). For routine clinical CT arthrography of the knee, typically 35 to 50 mL of total volume is injected[26] and 50% to 100% of the total volume can consist of iodinated contrast.[27] Compared with other exogenous CEST MRI applications, where contrast is injected intravenously and must permeate the tissue of interest, the diarthrodial joint may be unique in that direct administration of contrast is relatively easy and commonly performed. Much higher local contrast concentrations and therefore higher CEST effects would be expected compared with intravenous administration of contrast.

Clinically compatible pHe-sensitive imaging techniques have received increasing interest in recent years, and a number of techniques have been explored, including optical imaging techniques,[28] positron emission tomography,[29] and multinuclear MR spectroscopy.[30] However, each of these techniques has practical limitations for in vivo translation,

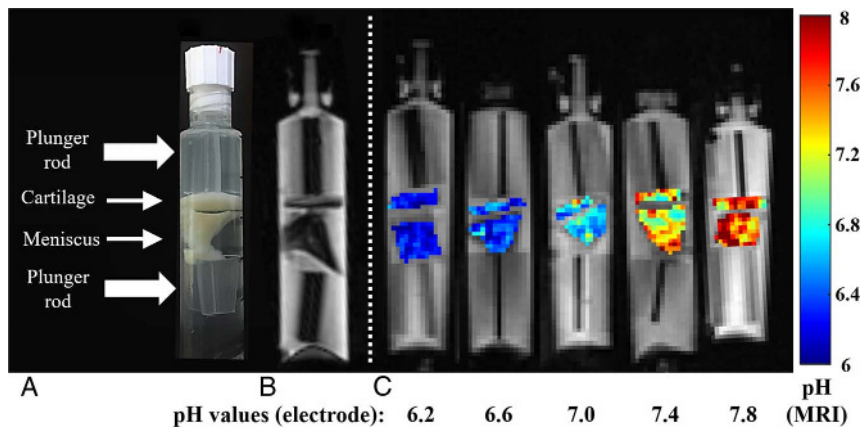

FIGURE 5. Phantoms containing both cartilage and meniscus immersed in 200 mM iohexol with varying pH, confirmed using an electrode. The pH maps are calculated based on the RPM fitting method for iohexol at 35°C. The construction of the tissue phantom is demonstrated with a photograph (A) and on a 3D fast spin echo image (B). Pixel-wise pH maps of both cartilage and meniscus (C) are shown with the corresponding fluid pH values ranging from 6.2 to 7.8. The pH calibration was derived from the fluid inside of the phantom.

including depth limitations, requirements for radioactive compounds produced by cyclotrons, and limited spatial resolution, respectively. Other pHe-sensitive MRI techniques also exist, including gagCEST[31] and R1ρ dispersion[32]; however, these may be less suitable for pH measurement of joint tissues because they are both sensitive to changes in tissue composition, such as glycosaminoglycans.[33,34] The acidoCEST technique overcomes most of these limitations. Specifically, the whole joint can be imaged with sufficient spatial resolution to identify individual joint structures; iohexol and iopamidol are available off-the-shelf, and both are already approved for intra-articular administration. Furthermore, pHe imaging with acidoCEST is not confounded by variations in local glycosaminoglycan concentration.[31]

A number of iodinated contrast agents have been used with the acidoCEST technique. However, to our knowledge, only iopamidol has been investigated on a 3 T clinical scanner.[17,35] Using the acidoCEST-UTE technique at 3 T, we compared iopromide, iohexol, and iopamidol, and found that all 3 agents were sensitive to pH using one of the ratiometric approaches. Overall, our results are consistent with previous studies that have also found significant correlations between CEST ratios and pH with iopromide,[14,31,36] iopamidol,[25,36–38] and iohexol.[39] However, iopromide demonstrated the lowest CEST effects of the three. Similar to our results, Moon et al[36] performed a comparison between iopromide and iopamidol, and found lower CEST effect for both the 4.2 and 5.6 ppm peaks with iopromide compared with iopamidol.

Saturation powers ranging from 0.54 (300 degrees) to 1.1 μT (600 degrees) were used in our study, which is in range with previous 3 T acidoCEST studies that used saturation powers from 0.2 μT to 1.5 μT.[17,35] Although the saturation efficiency with the powers used in our study was sufficient to detect CEST effects in phantoms and in vivo, the larger CEST effect was seen with 1.1 μT irradiation over 0.54 μT, as expected. When using a knee coil for RF transmission, even higher powers than 1.1 μT can be used while still operating with specific absorption rate limitations.[34] When using higher powers, however, other considerations such as increasing contributions from magnetization transfer[40] or broadening resulting in inadvertent saturation of other frequencies should be kept in mind.

We also examined several other variables that affect pH quantification, including contrast concentration, buffer type, and temperature. For the range of contrast concentrations used in this experiment (30 to 300 mM), both iohexol and iopamidol with ratiometric analyses were concentration independent. Our results are similar to a number of previous studies, including Müller-Lutz et al[35] who found that iopamidol was concentration-independent when imaged at 3 T over a range of 20 to 160 mM. Buffers should be considered for CEST experiments because they can potentially alter exchange rates in a complex manner.[41] The mechanism is not fully understood, but the effect can differ between exchange sites present on the same molecule.[42] Our results suggest that the presence and concentration of phosphate buffer does not significantly alter CEST effects or ratiometric analyses at the amide group peaks on iohexol or iopamidol. With regards to temperature, higher temperatures increase water exchange rates, resulting in broader CEST peaks.[43] The effect on CEST effect depends in part on the exchange rate at a particular field strength and can also differ between exchange sites present on the same molecule.[43,44] Overall, our results indicate that CEST effects increased from room temperature to 35°C for iohexol and iopamidol at the 4.2 ppm peak, but mildly decreased for the 5.6 ppm peak on iopamidol. Our iopamidol results are similar to those reported by Moon et al.[36] Ratiometric analyses differed between the 2 temperatures; however, confirming that calibration with pH should be made at the appropriate temperature.

In addition to the conventional ST ratiometric approach, we used the RF power-based ratiometric approach as described by Longo et al.[24] For iopamidol, we found comparable performance of the ST ratio compared with the RF power-based ratio at 4.2 ppm. However, iohexol contains only a single set of amide protons, and therefore can only be analyzed using the RF power-based ratiometric approach. Overall, our results suggest that iohexol is the preferred agent because the strongest correlation coefficients between ratiometric analyses and pH were seen. Furthermore, an important consideration that supports the use of iohexol is the very similar ratiometric (RPM) values between liquid, cartilage, and meniscus. Use of a single pH calibration scale that is composition independent would facilitate interpretation. Longo et al[37] found that RST after iopamidol administration yielded similar values between liquid and tumor homogenate. The differences in our results may be related to differences in scanner performance (preclinical vs clinical) or in tissue composition (homogenized tumor vs solid musculoskeletal tissue).

Our study has several limitations. First, our ex vivo tissues were soaked for 96 hours to ensure homogeneous contrast diffusion and pH equilibration based on prior literature.[45] Notable differences in vivo exist, including considerably shorter times for contrast penetration. Specifically, contrast flux is greatly accelerated with mechanical convection, and adequate contrast penetration could be expected in as short as 1 hour in a patient who is mobile,[46] particularly with nonionic contrast agents such as those used in our study.[47] Furthermore, local pH would be expected to be maintained in the in vivo condition. Chen et al[14] previously demonstrated that the pH of the injection solution did not influence the tumor tissue pH measurement when performed in vivo. In the joint, pH of tissue extracellular matrix is maintained by resident cells such as chondrocytes, and is typically lower than that of synovial fluid.[6] Second, the scan time for the acidoCEST-UTE technique is long, in part due to the use of multiple RF irradiation powers. However, for future in vivo studies, it would be recommended that the total number of datasets be lowered, focused near the frequencies of the CEST effect (±4.3 ppm in the case of iohexol). In addition, other opportunities for acceleration exist, including smaller coverage in the patient's location of pain, increasing the number of Cones spokes per preparation,[22] and utilization of parallel imaging or compressed sensing reconstruction. Third, an alternative method of data analysis involves fitting of the CEST spectra using Bloch equations modified for chemical exchange. Although this has been reported to be superior to ratiometric analyses,[17] unfortunately many more datasets are required over ratiometric approaches. Therefore, this is less suited for in vivo imaging of the knee using 3D sequences. Fourth, CEST techniques are expected to perform better at higher field strengths, and future experiments should consider use of 7 T scanners, which are now available for human use.[48,49] Finally, our technique was used on ex vivo tissue only, and we have not yet translated the acidoCEST-UTE technique in humans. However, due to the large number of considerations examined in this study, identification of the best contrast agent and technique variables before human use is mandatory. In an upcoming experiment, we plan to perform the technique in subjects who will undergo subsequent total knee replacement, thus providing the opportunity to correlate MR and electrode pH measurements as well as potentially demonstrate the significance of the pH measurement.

In conclusion, measuring pHe in cartilage and meniscus using acidoCEST-UTE MRI is feasible.

REFERENCES

1. Hunter DJ, Schofield D, Callander E. The individual and socioeconomic impact of osteoarthritis. *Nat Rev Rheumatol*. 2014;10:437–441.
2. Hayashi D, Roemer FW, Jarraya M, et al. Imaging in osteoarthritis. *Radiol Clin North Am*. 2017;55:1085–1102.
3. Chang EY, Ma Y, Du J. MR parametric mapping as a biomarker of early joint degeneration. *Sports Health*. 2016;8:405–411.
4. Loeser RF, Goldring SR, Scanzello CR, et al. Osteoarthritis: a disease of the joint as an organ. *Arthritis Rheum*. 2012;64:1697–1707.
5. Yusuf E, Kortekaas MC, Watt I, et al. Do knee abnormalities visualised on MRI explain knee pain in knee osteoarthritis? A systematic review. *Ann Rheum Dis*. 2011;70:60–67.

6. Smith DW. Cartilage tissue homeostasis. In: Smith DW, Gardiner BS, Zhang L, et al., eds. *Articular Cartilage Dynamics*. New York, NY: Springer Berlin Heidelberg; 2018:65–243.
7. Murphy G, Lee MH. What are the roles of metalloproteinases in cartilage and bone damage? *Ann Rheum Dis*. 2005;64(suppl 4):iv44–iv47.
8. Razaq S, Wilkins RJ, Urban JP. The effect of extracellular pH on matrix turnover by cells of the bovine nucleus pulposus. *Eur Spine J*. 2003;12:341–349.
9. Konttinen YT, Mandelin J, Li TF, et al. Acidic cysteine endoproteinase cathepsin K in the degeneration of the superficial articular hyaline cartilage in osteoarthritis. *Arthritis Rheum*. 2002;46:953–960.
10. Blair HC. How the osteoclast degrades bone. *Bioessays*. 1998;20:837–846.
11. Walsh DA, McWilliams DF, Turley MJ, et al. Angiogenesis and nerve growth factor at the osteochondral junction in rheumatoid arthritis and osteoarthritis. *Rheumatology (Oxford)*. 2010;49:1852–1861.
12. Abdelhamid RE, Sluka KA. ASICs mediate pain and inflammation in musculoskeletal diseases. *Physiology (Bethesda)*. 2015;30:449–459.
13. Deval E, Lingueglia E. Acid-sensing ion channels and nociception in the peripheral and central nervous systems. *Neuropharmacology*. 2015;94:49–57.
14. Chen LQ, Howison CM, Jeffery JJ, et al. Evaluations of extracellular pH within in vivo tumors using acidoCEST MRI. *Magn Reson Med*. 2014;72:1408–1417.
15. Ward KM, Balaban RS. Determination of pH using water protons and chemical exchange dependent saturation transfer (CEST). *Magn Reson Med*. 2000;44: 799–802.
16. Lindeman LR, Randtke EA, High RA, et al. A comparison of exogenous and endogenous CEST MRI methods for evaluating in vivo pH. *Magn Reson Med*. 2018; 79:2766–2772.
17. Jones KM, Randtke EA, Yoshimaru ES, et al. Clinical translation of tumor acidosis measurements with acidoCEST MRI. *Mol Imaging Biol*. 2017;19:617–625.
18. Goodwin DW. MR imaging of the articular cartilage of the knee. *Semin Musculoskelet Radiol*. 2009;13:326–339.
19. Goodwin DW, Wadghiri YZ, Zhu H, et al. Macroscopic structure of articular cartilage of the tibial plateau: influence of a characteristic matrix architecture on MRI appearance. *AJR Am J Roentgenol*. 2004;182:311–318.
20. Chang EY, Du J, Chung CB. UTE imaging in the musculoskeletal system. *J Magn Reson Imaging*. 2015;41:870–883.
21. Gurney PT, Hargreaves BA, Nishimura DG. Design and analysis of a practical 3D cones trajectory. *Magn Reson Med*. 2006;55:575–582.
22. Ma YJ, Chang EY, Carl M, et al. Quantitative magnetization transfer ultrashort echo time imaging using a time-efficient 3D multispoke cones sequence. *Magn Reson Med*. 2018;79:692–700.
23. Zu Z, Li K, Janve VA, et al. Optimizing pulsed-chemical exchange saturation transfer imaging sequences. *Magn Reson Med*. 2011;66:1100–1108.
24. Longo DL, Sun PZ, Consolino L, et al. A general MRI-CEST ratiometric approach for pH imaging: demonstration of in vivo pH mapping with iobitridol. *J Am Chem Soc*. 2014;136:14333–14336.
25. Longo DL, Dastru W, Digilio G, et al. Iopamidol as a responsive MRI-chemical exchange saturation transfer contrast agent for pH mapping of kidneys: in vivo studies in mice at 7 T. *Magn Reson Med*. 2011;65:202–211.
26. Chung CB, Isaza IL, Angulo M, et al. MR arthrography of the knee: how, why, when. *Radiol Clin North Am*. 2005;43:733–746, viii–ix.
27. Kalke RJ, Di Primio GA, Schweitzer ME. MR and CT arthrography of the knee. *Semin Musculoskelet Radiol*. 2012;16:57–68.
28. Schreml S, Meier RJ, Wolfbeis OS, et al. 2D luminescence imaging of pH in vivo. *Proc Natl Acad Sci U S A*. 2011;108:2432–2437.
29. Vavere AL, Biddlecombe GB, Spees WM, et al. A novel technology for the imaging of acidic prostate tumors by positron emission tomography. *Cancer Res*. 2009; 69:4510–4516.
30. Miloushev VZ, Keshari KR, Holodny AI. Hyperpolarization MRI: preclinical models and potential applications in neuroradiology. *Top Magn Reson Imaging*. 2016;25:31–37.
31. Melkus G, Grabau M, Karampinos DC, et al. Ex vivo porcine model to measure pH dependence of chemical exchange saturation transfer effect of glycosaminoglycan in the intervertebral disc. *Magn Reson Med*. 2014;71:1743–1749.
32. Zu Z, Li H, Jiang X, et al. Spin-lock imaging of exogenous exchange-based contrast agents to assess tissue pH. *Magn Reson Med*. 2018;79:298–305.
33. Wang P, Block J, Gore JC. Chemical exchange in knee cartilage assessed by R1ρ (1/T1ρ) dispersion at 3T. *Magn Reson Imaging*. 2015;33:38–42.
34. Singh A, Haris M, Cai K, et al. Chemical exchange saturation transfer magnetic resonance imaging of human knee cartilage at 3 T and 7 T. *Magn Reson Med*. 2012;68:588–594.
35. Müller-Lutz A, Khalil N, Schmitt B, et al. Pilot study of iopamidol-based quantitative pH imaging on a clinical 3T MR scanner. *MAGMA*. 2014;27:477–485.
36. Moon BF, Jones KM, Chen LQ, et al. A comparison of iopromide and iopamidol, two acidoCEST MRI contrast media that measure tumor extracellular pH. *Contrast Media Mol Imaging*. 2015;10:446–455.
37. Longo DL, Bartoli A, Consolino L, et al. In vivo imaging of tumor metabolism and acidosis by combining PET and MRI-CEST pH imaging. *Cancer Res*. 2016;76:6463–6470.
38. Wu Y, Zhou IY, Igarashi T, et al. A generalized ratiometric chemical exchange saturation transfer (CEST) MRI approach for mapping renal pH using iopamidol. *Magn Reson Med*. 2018;79:1553–1558.
39. Longo DL, Michelotti F, Consolino L, et al. In vitro and in vivo assessment of nonionic iodinated radiographic molecules as chemical exchange saturation transfer magnetic resonance imaging tumor perfusion agents. *Invest Radiol*. 2016;51: 155–162.
40. Desmond KL, Stanisz GJ. Understanding quantitative pulsed CEST in the presence of MT. *Magn Reson Med*. 2012;67:979–990.
41. Liepinsh E, Otting G. Proton exchange rates from amino acid side chains—implications for image contrast. *Magn Reson Med*. 1996;35:30–42.
42. Ward KM, Aletras AH, Balaban RS. A new class of contrast agents for MRI based on proton chemical exchange dependent saturation transfer (CEST). *J Magn Reson*. 2000;143:79–87.
43. van Zijl PC, Yadav NN. Chemical exchange saturation transfer (CEST): what is in a name and what isn't? *Magn Reson Med*. 2011;65:927–948.
44. Sheth VR, Liu G, Li Y, et al. Improved pH measurements with a single PARACEST MRI contrast agent. *Contrast Media Mol Imaging*. 2012;7:26–34.
45. Silvast TS, Kokkonen HT, Jurvelin JS, et al. Diffusion and near-equilibrium distribution of MRI and CT contrast agents in articular cartilage. *Phys Med Biol*. 2009; 54:6823–6836.
46. Entezari V, Bansal PN, Stewart RC, et al. Effect of mechanical convection on the partitioning of an anionic iodinated contrast agent in intact patellar cartilage. *J Orthop Res*. 2014;32:1333–1340.
47. Yoo HJ, Hong SH, Choi JY, et al. Contrast-enhanced CT of articular cartilage: experimental study for quantification of glycosaminoglycan content in articular cartilage. *Radiology*. 2011;261:805–812.
48. Friebe B, Richter M, Penzlin S, et al. Assessment of low-grade meniscal and cartilage damage of the knee at 7 T: a comparison to 3 T imaging with arthroscopic correlation. *Invest Radiol*. 2018;53:390–396.
49. Springer E, Bohndorf K, Juras V, et al. Comparison of routine knee magnetic resonance imaging at 3 T and 7 T. *Invest Radiol*. 2017;52:42–54.